Specificity Determinants of Human Cathepsin S Revealed by Crystal Structures of Complexes[†,‡]

Thomas A. Pauly,[§] Traian Sulea,[||] Mark Ammirati,[§] J. Sivaraman,[||] Dennis E. Danley,[§] Matthew C. Griffor,[§] Ajith V. Kamath,[§,⊥] I.-K. Wang,[§] Ellen R. Laird,[§] Andrew P. Seddon,[§] Robert Ménard,[||] Miroslaw Cygler,*[,||] and Virginia L. Rath*[,§,#]

Exploratory Medicinal Sciences and Computational Chemistry, Groton Laboratories, Pfizer Global Research and Development, Eastern Point Road, Groton, Connecticut 06340, and Biotechnology Research Institute, 6100 Royalmount Avenue, Montreal, Quebec H4P 2R2, Canada

Received December 5, 2002; Revised Manuscript Received January 23, 2003

ABSTRACT: Cathepsin S, a lysosomal cysteine protease of the papain superfamily, has been implicated in the preparation of MHC class II $\alpha\beta$-heterodimers for antigen presentation to CD4+ T lymphocytes and is considered a potential target for autoimmune-disease therapy. Selective inhibition of this enzyme may be therapeutically useful for attenuating the hyperimmune responses in a number of disorders. We determined the three-dimensional crystal structures of human cathepsin S in complex with potent covalent inhibitors, the aldehyde inhibitor 4-morpholinecarbonyl-Phe-(*S*-benzyl)Cys-Ψ(CH=O), and the vinyl sulfone irreversible inhibitor 4-morpholinecarbonyl-Leu-Hph-Ψ(CH=CH−SO_2−phenyl) at resolutions of 1.8 and 2.0 Å, respectively. In the structure of the cathepsin S−aldehyde complex, the tetrahedral thiohemiacetal adduct favors the *S*-configuration, in which the oxygen atom interacts with the imidazole group of the active site His164 rather than with the oxyanion hole. The present structures provide a detailed map of noncovalent intermolecular interactions established in the substrate-binding subsites S3 to S1′ of cathepsin S. In the S2 pocket, which is the binding affinity hot spot of cathepsin S, the Phe211 side chain can assume two stable conformations that accommodate either the P2-Leu or a bulkier P2-Phe side chain. This structural plasticity of the S2 pocket in cathepsin S explains the selective inhibition of cathepsin S over cathepsin K afforded by inhibitors with the P2-Phe side chain. Comparison with the structures of cathepsins K, V, and L allows delineation of local intermolecular contacts that are unique to cathepsin S.

Cathepsin S is a lysosomal cysteine protease that has been found to be predominantly expressed in antigen presenting cells (i.e., macrophages, B cells, and dendritic cells (*1*−*3*)). Experiments using protease inhibitors (*4*) and knockout mice (*5*, *6*) have clearly shown that cathepsin S is involved in processing of the invariant chain (Ii), a necessary event in order for the cells to be able to present the antigens at their surface, and is therefore implicated in the process of MHC class II antigen presentation. More recently, it was demonstrated that cathepsin S also plays a role in processing of the antigen for presentation on MHC class II molecules (*7*). The finding that cathepsin S, and a few other enzymes such as cathepsins L (*8*) and possibly F (*9*), are responsible for critical steps in antigen presentation raises the possibility that a specific inhibition of these proteases may be beneficial for the treatment of various diseases with elevated immune responses, such as asthma, transplant rejection, and autoimmune disorders. It has also been speculated, based on the observation that cathepsin S is present in the lung and has high elastinolytic activity, that cathepsin S can play a role in emphysema (*10*).

Cathepsin S belongs to Clan C1 cysteine proteases (*11*). Several human homologues of cathepsin S are found in Clan C1. These enzymes share a basic endopeptidase platform composed of a papain-like two-domain protein, with the substrate binding site located in the inter-domain cleft (*12*, *13*). A few members (cathepsins B, C, H, and X) are designed to act as exopeptidases and have additional structural features that define substrate specificity and can be utilized for selective binding of ligands and inhibitors. For the endopeptidases however, and in particular cathepsins K, L, S, and V, functional diversity in ligand recognition is subtler. Indeed, substrate specificity for this group of enzymes is considered to be relatively broad, with the nature of the residue at position P2 of a substrate being in many cases the most significant specificity determinant (*14*). Designing a ligand that could specifically inhibit only one enzyme of this group, in the present case cathepsin S, represents a challenging task and an important issue for the development of an effective drug for the treatment of diseases related to cathepsin S. The availability of crystal structures for endopeptidases complexed with ligands is definitively

[†] NRCC publication No. 46167.

[‡] The atomic coordinates and observed structure factors have been deposited with the Protein Data Bank (entries 1NPZ and 1NQC).

* To whom correspondence should be addressed. (V.L.R.) Tel.: (510) 420-6714. Fax: (510) 420-6795. E-mail: virginiar@thiospharm.com. (M.C.) Tel.: (514) 496-6321. Fax: (514) 496-5143. E-mail: mirek@bri.nrc.ca.

[§] Pfizer Global Research and Development.

[||] Biotechnology Research Institute.

[⊥] Current address: Discovery Technology Center, Pfizer Global Research and Development, 620 Memorial Drive, Cambridge, MA 02139.

[#] Current address: Thios Pharmaceuticals, 5980 Horton St., Suite 400, Emeryville, CA 94608.

10.1021/bi027308i CCC: $25.00
Published on Web 02/25/2003

of great value to assist in structure-based molecular design and/or optimization of an immunosuppressive drug acting as a specific cathepsin S inhibitor.

Although two crystal structures of human cathepsin S have been reported in the literature, both lack important information necessary for structure-based design of specific inhibitors. In the 2.5-Å resolution structure of cathepsin S cocrystallized with a potent irreversible vinyl sulfone inhibitor (*15*), a number of structural features of the substrate-binding subsites of the enzyme could not be delineated. Most of the missing structural details are precisely those associated with putative binding affinity and/or specificity hot spots of cathepsin S. In addition, the structure is not publicly available. The more recent 2.2-Å resolution crystal structure of the inhibitor-free, inactive Cys25Ser mutant of cathepsin S (*16*) does not provide information about the protein−inhibitor interactions.

In this work, the crystallographic structures of mature human cathepsin S in complex with the aldehyde inhibitor, Mu-Phe-(SBz)Cys-Ψ(CH═O),[1] and the vinyl sulfone inhibitor, Mu-Leu-Hph-Ψ(CH═CH−SO_2−Ph), were determined at a resolution of 1.8 and 2.0 Å, respectively. These potent inhibitors of cathepsin S constitute suitable molecular probes for mapping intermolecular interactions at the substrate-binding subsites of the enzyme. In addition, although the reactive groups of these inhibitors are different, their chemical structures nicely complement each other in that they contain a common peptidic scaffold with different side chains expected to interact at a given subsite of the enzyme. Known inhibition constants for cathepsins S, K, and L (*17*) facilitate delineation of binding specificity determinants across these closely related endopeptidases. Moreover, the crystal structures of human cathepsin K and human cathepsin V (a very close homologue of cathepsin L) complexed with vinyl sulfone analogues have been reported (*18*, *19*). We will present a detailed comparative analysis of the covalent and noncovalent intermolecular interactions of the inhibitors in the substrate-binding cleft of cathepsin S. The quality of the structural data reported here allows identification of structural features of cathepsin S subsites that could be exploited in further structure-based therapeutic efforts toward development of highly specific inhibitors of this enzyme.

EXPERIMENTAL PROCEDURES

Construction of Expression Vector. The signal sequence from the suc2 gene was subcloned from a plasmid pHIL-S1suc2 into pPICZ (Invitrogen, Carlsbad, CA). The cDNA fragment coding for peptide Gln17-Ile331 of cathepsin S was amplified by PCR using a clone that secretes cathepsin S as template (unpublished data). The following primers were used for PCR: 5′-GCGATATCTGCTCAGTTGCATAAAGATCCT-3′ (*Eco*RV) and 5′-CGGGATCCTCTAGATTTCTGGGTAAG-3′ (*Xba*I). The PCR was performed using Expand High Fidelity PCR System (Roche Diagnostics, Indianapolis, IN) with an initial denaturation of 94 °C for 2 min followed by 35 cycles of 94 °C for 15 s, 56 °C for 30 s, and 68 °C for 1 min followed by a final extension of 68 °C for 4 min. The 966 bp PCR product was digested with *Eco*RV and *Xba*I. A plasmid containing the *Saccharomyces cerevisiae* invertase SUC2 signal sequence was digested with *Nsi*I and *Eco*RV. pPICZαA (Invitrogen) was digested with *Nsi*I and *Xba*I. These three DNA fragments were used in a three-way ligation with the Rapid DNA Ligation Kit (Roche Diagnostics) to yield a construct expressing the first 19 amino acids of the SUC2 gene fused to amino acids 17−331 of cathepsin S. This construct was named pPICZSUC2CatS (pMCG29).

Transformation and Screening of Pichia pastoris. P. pastoris strain KM71 was transformed by electroporation using an Electro Cell Manipulator ECM600 (Genetronics, Inc., San Diego, CA) according to the protocol supplied from Genetronics (BTX-PRO250). pPICZSUC2CatS (pMCG29) was linearized with *Sac*I, and 10 μg of DNA was used to transform 80 μL of electrocompetent KM71 in 2 mm gap cuvettes. Cells were plated onto YPDS plates (1% yeast extract, 2% peptone, 2% dextrose, 1 M sorbitol, and 2% agar) containing 100 μg/mL Zeocin (Invitrogen). Individual colonies were screened for expression after growth for 72 h in BMMY media (1% yeast extract, 2% peptone, 100 mM potassium phosphate, pH 6.0, 1.34% yeast nitrogen base w/o amino acids, 4×10^{-5}% biotin, and 0.5% methanol). Culture supernatants were analyzed by Western blot using a polyclonal anti-cathepsin S antibody (kindly supplied by W. Brissette, Pfizer, Inc.). A single clone was used for shake flask experiments, which yielded 2.9 mg/L of mature cathepsin S.

Fermentation. The culture was grown in a 5 L glass fermentor (New Brunswick Scientific, Edison, NJ) with 3.5 L of minimal medium (Invitrogen) buffered with 300 mM phosphate, pH 5.5. The medium was supplemented with biotin (8×10^{-5}%), glucose (0.33%), and yeast extract (0.2%) along with 1 mL/L of Pichia trace metals (PTM1). The temperature was controlled at 25 °C and the agitation maintained at 450 rpm, but the pH was not controlled. A total of 35 mL of culture grown overnight in YPD (24 °C, 17 optical density units at 600 nm) was used to inoculate 3.5 L of fermentation medium. At 23 h post inoculation, methanol induction was commenced whereby methanol, supplemented with 12 mL/L PTM1, was fed to the reactor to a final concentration of 0.5% (v/v). Thereafter, the methanol was maintained at 0.4% (v/v) using the closed-loop control system based on the feedback signal provided by the methanol sensor (Raven Biotech, Vancouver, BC). At 143 h after induction, the supernatant from a 4 L culture yielded 2.24 mg/L of mature cathepsin S after cation exchange column.

Purification of Human Cathepsin S. The expressed procathepsin S was secreted to the medium. Yeast cells in culture were centrifuged at 4000*g* for 15 min, and the supernatant was concentrated to 140 mL using a TCF-10 ultrafiltration system equipped with an Amicon YM10 membrane. The concentrated solution was diafiltered against 20 mM sodium acetate, 5 mM DTT, 5 mM EDTA, pH 5.0 to allow autoprocessing of the proenzyme (1 h at 30 °C). The mixture containing the processed enzyme was applied on an SP-Sepharose column (2.6 × 20 cm) equilibrated with 20 mM sodium acetate buffer, pH 5.0. Elution was carried out using a linear gradient from 0 to 1 M NaCl, in 50 mM sodium acetate buffer, pH 5.0. Mature cathepsin S eluted at approximately 0.3 M NaCl. The enzyme was then reversibly

[1] Abbreviations: Mu, *N*-morpholinecarbonyl; Hph, homophenylalanine; (SBz)Cys, *S*-benzyl-cysteine; Ph, phenyl.

inhibited by adding 0.1 mM MMTS (methyl methanethiolsulfonate). This sample was then concentrated and further purified on a 1.6 × 60 cm Superdex 75 column (Pharmacia). Purified cathepsin S was eluted with 50 mM acetate and 0.2 M NaCl, pH 5.0 buffer. As a precautionary measure, 0.1 mM MMTS was added to the purified sample, and the enzyme was stored in the inhibited form at 4 °C.

Crystallization of Cathepsin S Complexes. Cathepsin S was concentrated and exchanged into 20 mM sodium acetate pH 5.5−6.0 at 3 mg/mL (0.12 mM). The enzyme was activated with 1−2 mM DTT. The vinyl sulfone inhibitor morpholine-4-carboxylic acid [1-(3-benzenesulfonyl-1-phenethyl-allylcarbamoyl)-3-methyl-butyl]-amide was synthesized by S. A. Eisenbeis at Groton Laboratories, Pfizer, Inc., while the aldehyde inhibitor morpholine-4-carboxylic acid [1-(2-benzylsulfanyl-1-formyl-ethylcarbamoyl)-2-phenyl-ethyl]-amide was synthesized by Enzyme Systems Products (Livermore, CA).

The vinyl sulfone inhibitor complex was formed by the mixing activated protein diluted to 0.25 mg/mL (10 μM) with inhibitor from DMSO stock to a final concentration of 0.4 mM and 0.12% DMSO. The sample was diluted 1:10 with 20 mM sodium acetate, pH 6.0, to dilute the DMSO to 0.012%, followed by a final concentration to 10.2 mg/mL. Microcrystals were grown at 22 °C by the hanging drop vapor diffusion method. Drops were made with 2 μL of inhibited protein at 10.2 mg/mL plus 2 μL of reservoir solution containing 0.1 M sodium cacodylate pH 6.5, 0.2 M ammonium sulfate, and 20% PEG 4000. These microcrystals were streak seeded into preequilibrated drops that were made using 2 μL of the same protein−inhibitor complex plus 2 μL of reservoir containing 0.1 M sodium acetate pH 4.6, 0.2 M ammonium sulfate, and 10% PEG 4000. Crystals grew to 100 × 100 × 50 μm. The data from these crystals was measured at room temperature using a rotating anode source and a Mar 300 detector. All data were reduced and scaled with DENZO and SCALEPACK (*20*).

The aldehyde inhibitor complex was formed from a mixture protein at concentration of 0.40 mg/mL (16.2 μM), 0.22 mM inhibitor, and 0.22% DMSO. The inhibited protein was concentrated to 10.8 mg/mL. Crystals were grown in hanging drops by the method of vapor diffusion at 22 °C. Drops were formed with 2 μL of protein plus 1.6 μL of buffer containing 0.125 M sodium acetate pH 5.5, 1.5 M ammonium sulfate, and 0.4 μL of 10% methylpentanediol, with 1% MPD added. The drops were equilibrated over a reservoir containing 0.1 M sodium acetate, pH 5.5, and 1.2 M ammonium sulfate. Crystals grew to 100 × 250 × 50 μm. Prior to data measurement, these crystals were transferred in a stepwise procedure to a cryo-stabilization solution of 0.1 M sodium acetate, pH 5.5, 1.2 M lithium sulfate, and 5% glycerol and then flash frozen in liquid propane and stored under liquid nitrogen. The data were measured at beamline 5.0.2 at the Advanced Light Source (Berkeley, CA) at 100 K. All data were reduced and scaled with DENZO and SCALEPACK (*20*).

Structure Solution and Refinement. The structure of cathepsin S in complex with the aldehyde inhibitor was solved using molecular replacement in CNS (*21*). Although the structure of cathepsin S was already published (*15*), the coordinates were not released. Hence, our search model consisted of a polyalanine homology model of cathepsin S constructed from cathepsin K (PDB code 1atk) and cathepsin L from the pro-cathepsin L (PDB code 1cjl) using SYBYL 6.6 (Tripos, Inc., St. Louis, MO). Only one loop near the C-terminus was built from the coordinates of cathepsin L, and the rest of the model came from cathepsin K. The rotation search clearly showed one peak, which corresponded to one molecule in the asymmetric unit. The inhibitor structure was modeled into the map using the program O (*22*) and refined using CNS (*21*). After several cycles of map fitting and refinement, a final R factor of 19.9% (R_{free} = 21.9%) was obtained for all the reflections within the resolution range of 1.8−30.0 Å. The cathepsin S coordinates from this refined model were then taken for the structure solution of the inhibitor complex. The rotation search clearly showed two peaks corresponding to two molecules in the asymmetric unit. Model building and refinement resulted in the final R factor of 19.2% (R_{free} = 21.9%) for all the reflections within 2.0−30.0-Å resolution. The deviation of the model from ideal geometry was evaluated with PROCHECK (*23*). The details of data collection and refinement are given in Table 1.

Table 1: Crystallographic Data for Cathepsin S Complexes

data set	cathepsin S/ aldehyde	cathepsin S/ vinyl sulfone
Data Collection		
space group	$P2_12_12_1$	R_3
unit cell (Å)	a = 36.9	$a = b$ = 108.1
	b = 76.5	
	c = 101.9	c = 105.3
resolution range (Å)	30.0−1.8	30.0−2.0
observed *hkl*	207 486	83 669
unique *hkl*	25 170	30 379
completeness (%)	91.4	98.5
overall $I/\sigma I$	6.4	7.5
R_{sym} (%)	14.8	9.1
Refinement		
R_{free} (%)	21.9	21.9
R_{work} (%)	19.9	19.2
rmsd bond lengths (Å)	0.01	0.01
rmsd bond angles (deg)	1.4	1.5
mean coordinate error (Å)	0.2	0.23
Ramachandran Plot		
favored region (%)	86.7	85.9
allowed region (%)	13.3	13.8
generously allowed (%)	0.0	0.3
disallowed region (%)	0.0	0.0
Average B-factors (Å^2)		
main chain atoms (# atoms)	13.2 (863)	24.9 (1728)
side chain atoms (# atoms)	14.8 (818)	26.2 (1634)
overall protein (# atoms)	14.0 (1681)	25.5 (3362)
waters (# atoms)	28.5 (245)	35.8 (175)
ligand (# atoms)	20.8 (38)	20.9 (86)

RESULTS AND DISCUSSION

Selection of the Inhibitors. In this work, the crystallographic structures of mature human cathepsin S in complex with the aldehyde inhibitor, Mu-Phe-(SBz)Cys-Ψ(CH═O), and in complex with the vinyl sulfone inhibitor, Mu-Leu-Hph-Ψ(CH═CH−SO_2−Ph), were determined at 1.8 and 2.0 Å resolution, respectively. The chemical structures of the two inhibitors are drawn in Figure 1. Selection of these two compounds for cocrystallization and structure determination was motivated primarily by their high inhibitory potency against human cathepsin S. The aldehyde is a covalent

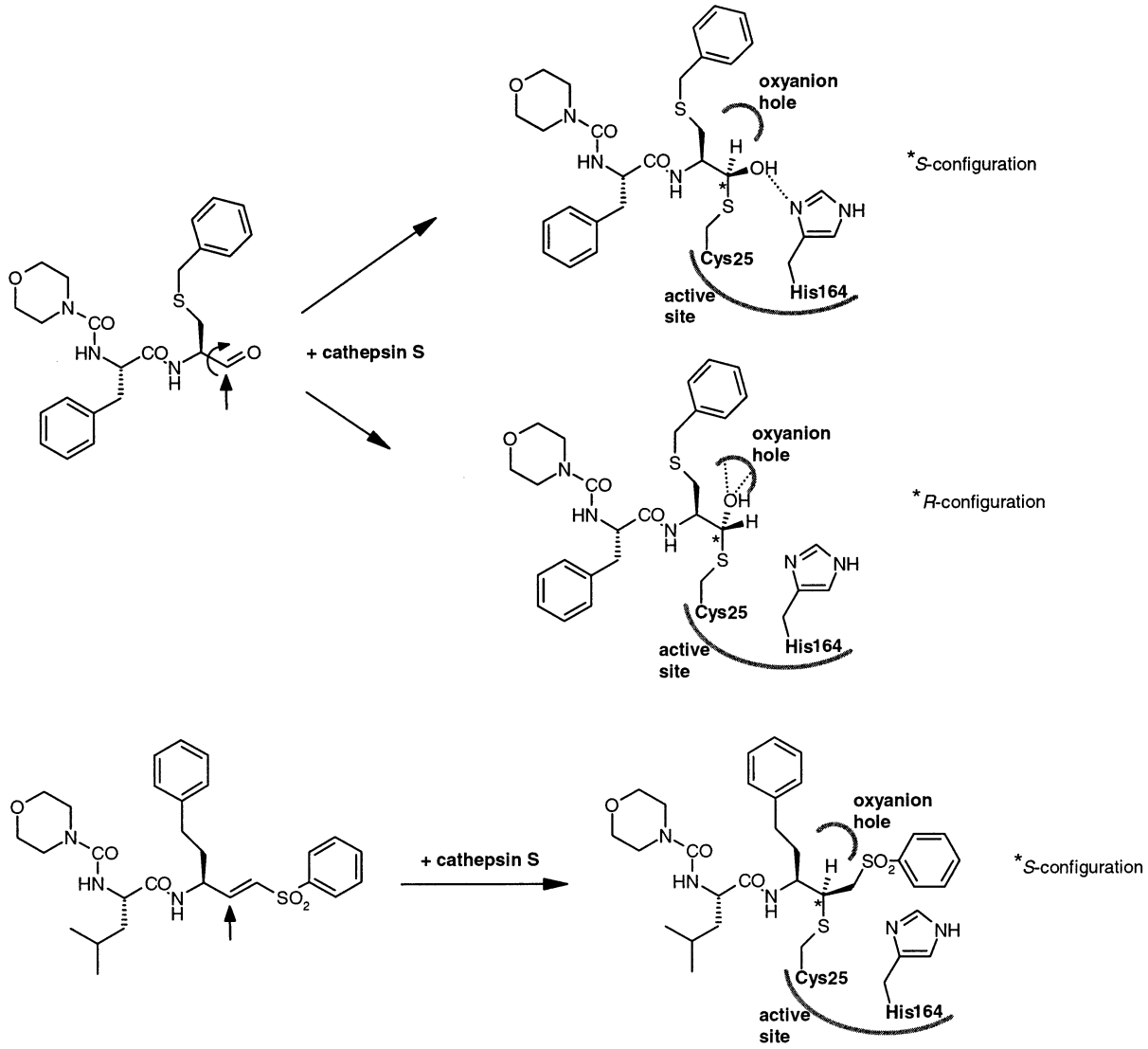

FIGURE 1: Chemical structures of the aldehyde inhibitor, morpholine-4-carboxylic acid [1-(2-benzylsulfanyl-1-formyl-ethylcarbamoyl)-2-phenyl-ethyl]-amide and of the vinyl sulfone inhibitor, morpholine-4-carboxylic acid [1-(3-benzenesulfonyl-1-phenethyl-allylcarbamoyl)-3-methyl-butyl]-amide, cocrystallized with cathepsin S. The position of the nucleophilic attack of the active site Cys25 thiolate of cathepsin S is indicated. Chemical structures of the formed enzyme−inhibitor adducts are shown on the right, with the emphasis on the observed stereochemistry, as well as on the interactions with the oxyanion hole and active site His164 of cathepsin S. All depicted interactions are between neutral species.

reversible inhibitor of human cathepsin S with an inhibition constant, K_i, of 50 nM. The vinyl sulfone inhibits irreversibly cathepsin S with a second-order rate constant of inactivation, k_{inact}/K_i, of 14.6×10^6 M^{-1} s^{-1} and a K_i of 13 nM (*17*). These inhibitors constitute suitable molecular probes for mapping intermolecular interactions at the substrate-binding subsites of the enzyme.

Overall Structure of the Enzyme. The structure of cathepsin S is nearly identical in the two inhibited complexes investigated here, with a root-mean-square deviation (rmsd) of 0.30 Å between the positions of equivalent main chain atoms of all the 217 amino acid residues of the enzyme. The overall fold of cathepsin S is very similar to that of other cysteine proteases of the papain superfamily. The cathepsin S structure superimposes onto the structures of cathepsins K, V, and L (endopeptidases) with rmsd values of 0.64−0.80 Å for more than 214 equivalent Cα atoms and onto the structures of cathepsins B, X, H, and C (exopeptidases) with rmsd values of 1.14−1.48 Å for more than 197 Cα-pairs (Figure 2). Thus, the architecture of the cathepsin S molecule is typical for a member of the papain superfamily of cysteine proteases and consists of two domains, the N-terminal domain dominated by α-helices and the C-terminal domain composed mainly of β-strands. Of the nine cysteine residues of the mature human cathepsin S, six are engaged in disulfide bridges that contribute to the overall stability of the folded structure. The unpaired Cys25 along with residues His164 and Asn184 form the catalytic triad, which is located at the interface between the two domains where a deep cleft extending on both sides of the active center forms the substrate-binding site. The open, unobstructed nature of the substrate-binding groove also classifies cathepsin S as an endopeptidase similar to cathepsins L, K, and V, as opposed to other members of the papain superfamily (e.g., cathepsins B, X, H, and C), which possess various exopeptidase activities because of structural features inserted on the common endopeptidase platform in the proximity of the active center.

Covalent Attachment of the Inhibitors. The electron density maps clearly indicate that both inhibitors bind covalently to cathepsin S (Figure 3). The peptidyl backbone of the

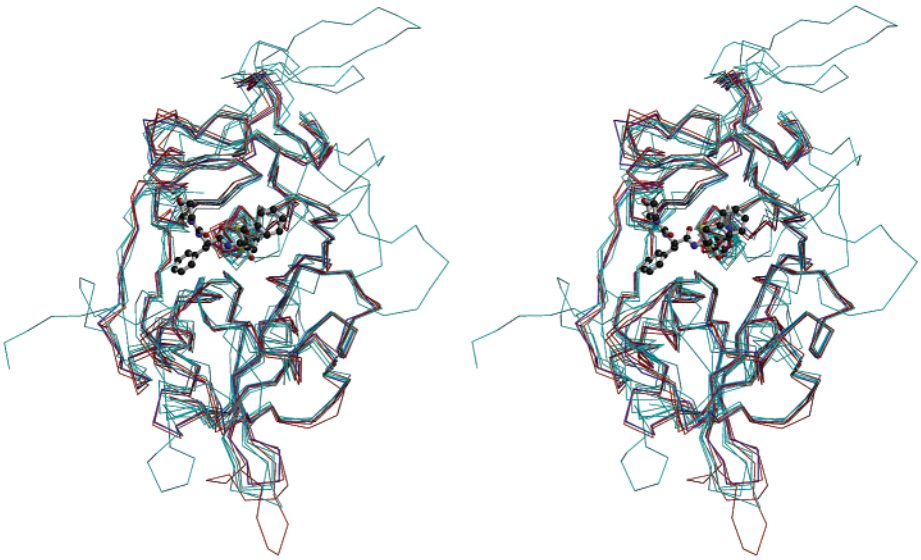

FIGURE 2: Stereoview of the three-dimensional superposition of the cathepsin S structure with the known structures of cysteine proteases of the papain superfamily. The structures of the eight superimposed enzymes are represented as Cα-trace and color-coded as follows: cathepsin S—blue; endopeptidases: cathepsins L (PDB code 1cs8), K (1mem), and V (1fh0)—red; and exopeptidases: cathepsins B (1csb), X (1deu), C (1k3b), and H (8pch)—cyan. The aldehyde inhibitor cocrystallized with cathepsin S is also displayed (ball-and-stick) and indicates the location of the substrate-binding cleft relative to the overall architecture of the enzyme.

inhibitors is oriented in the substrate-binding mode. The binding conformation of the inhibitors is not influenced by crystal contacts.

In the complex with the aldehyde inhibitor, a tetrahedral thiohemiacetal adduct is formed by the attack of the active site Cys25 thiolate nucleophile of the enzyme on the electrophilic sp^2 carbon of the inhibitor's reactive aldehyde, which changes to the sp^3 geometry. The electron density map shows clearly two orientations of the C-terminal hydroxyl of the inhibitor corresponding to either *S* or *R* absolute configuration of the tetrahedral thiohemiacetal adduct (Figures 1 and 3b). This would indicate that the aldehyde can bind the enzyme with the C-terminal carbonyl group in either of two conformations relative to the rest of the inhibitor, corresponding to a nucleophilic attack perpendicular to either side of the aldehyde plane. In the *S*-configuration, the oxygen atom of the adduct points toward the His164 of the active site and is positioned in the plane of the imidazole ring at the distance of 2.5 Å from the Nδ atom (Figure 3b). Such a short hydrogen bond would suggest an ion pair formation between the oxyanion and the protonated His164, although the proton transfer and the hydrogen bond interaction between the neutral species is also plausible. In the *R*-configuration, the oxygen atom of the adduct binds to the so-called oxyanion hole of the enzyme, where it forms hydrogen bonds with the side chain Nϵ atom of Gln19 and the main chain NH group of Cys25. The electron density for the *S*-configuration is stronger than for the *R*-configuration (see Figure 3b). Thus, we conclude that while both configurations populate the tetrahedral thiohemiacetal adduct, the *S*-configuration is preferentially stabilized.

This stereochemical preference of the tetrahedral thiohemiacetal adduct with the hydroxyl group interacting with the catalytic histidine rather than with the oxyanion hole has been postulated from mutagenesis experiments combined with kinetic analysis for papain inhibition by the aldehyde acetyl-Phe-Gly-Ψ(CH═O) (*24*). In that study, the oxyanion hole has been shown to be operational for stabilization of the transition state in substrate hydrolysis but not for stabilization of the tetrahedral thiohemiacetal adduct. Structurally, because the attacked carbonyl carbon of the substrate is substituted with the amide bond to be cleaved, and because of the steric restrictions imposed at the enzyme's active site, the transition state in the enzyme−substrate complex can be accommodated only in a unique configuration corresponding to the oxyanion interacting with the oxyanion hole. However, in the case of the aldehyde inhibitor, the small hydrogen atom attached to the attacked carbonyl carbon does not impede the rotation of the carbonyl group, which can bind in either of two conformations leading to the two absolute configurations of the formed tetrahedral adduct (Figure 1). The two conformations of the enzyme-bound aldehyde carbonyl could have similar stabilities, and the equilibrium between these conformations could be very sensitive to experimental conditions and might also be influenced by subtle structural differences between various cysteine proteases and aldehyde inhibitors. For example, in the papain structure complexed with the aldehyde inhibitor leupeptin, only the configuration of the thiohemiacetal with the oxygen atom interacting with the oxyanion hole was observed (*25*). However, in the aldehyde−cathepsin S complex investigated here, both conformations of the aldehyde carbonyl are present in the complex mixture, with preference toward the conformation leading to the *S*-configuration of the thiohemiacetal (i.e., with the hydroxyl group interacting with the catalytic histidine). Our structure provides direct physical evidence that, at least in some cases, the oxyanion hole is not important for aldehyde binding to cysteine proteases, in complete agreement with the biochemical data on aldehyde binding to papain (*24*). It is worth noting that a similar, limited contribution of the oxyanion hole can be found in aldehyde binding to serine proteases as well (*26*), as demonstrated, for example, by the crystal structure of the aldehyde inhibitor chymostatin in complex with the *Streptomyces griseus* protease A (*27*). In that case, it was shown that the formed hemiacetal populates equally

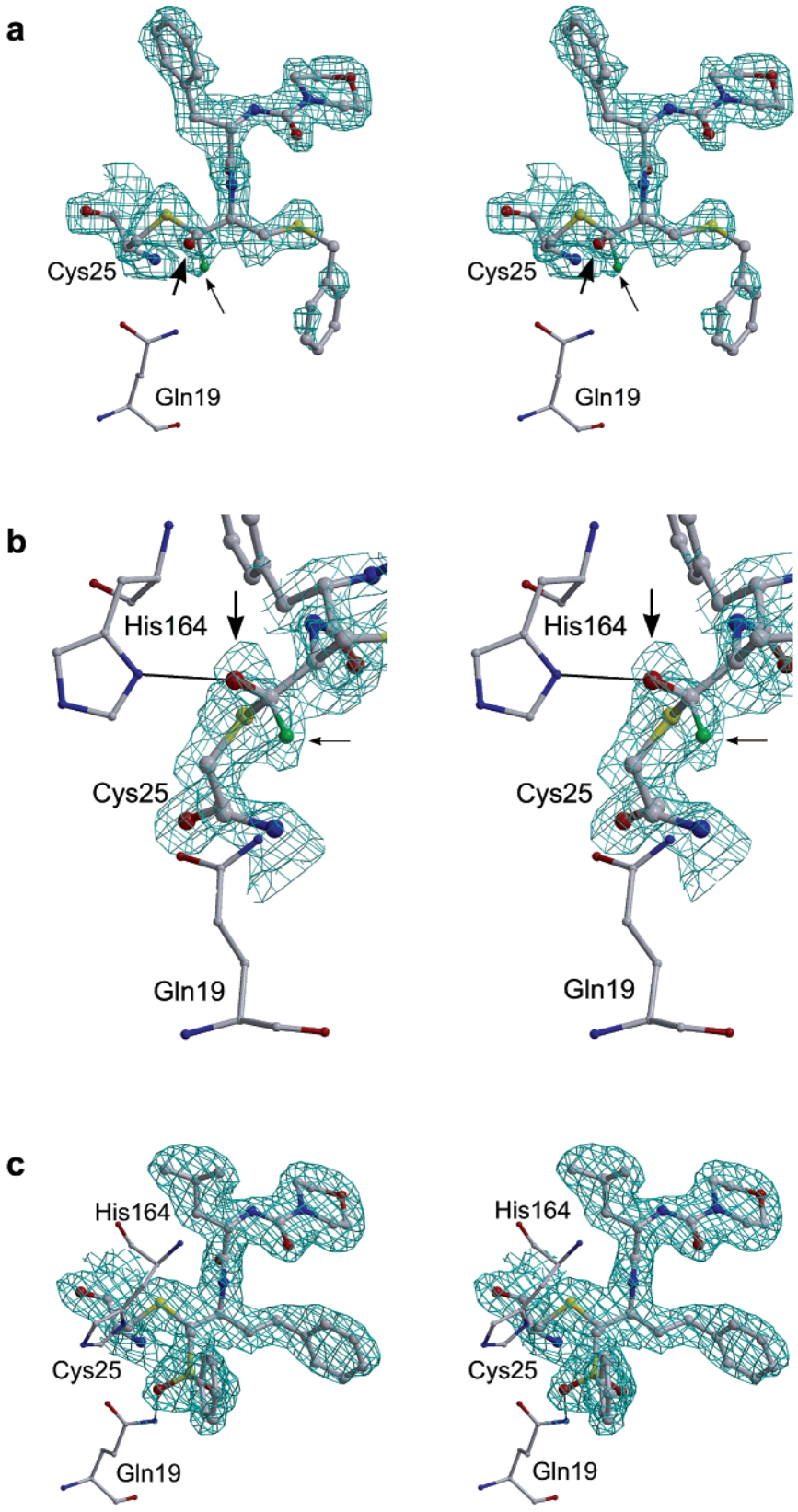

FIGURE 3: Stereoviews of the $F_o - F_c$ simulated annealing omit maps showing the electron density in the cathepsin S active site region. (a) Cathepsin S—aldehyde inhibitor complex. Panel b zooms in the region of the thiohemiacetal adduct formed between cathepsin S and the aldehyde inhibitor. Two alternate configurations of the tetrahedral adduct corresponding to two different orientations of the thiohemiacetal oxygen atom are modeled in the electron density map: the *S*-configuration (thick arrow) shown with a red oxygen atom, or the *R*-configuration (thin arrow) shown with a green oxygen atom. (c) Cathepsin S—vinyl sulfone inhibitor complex. For both complexes, all atoms of the inhibitor, the active site Cys25, and 3.5 Å around them were omitted prior to the map calculations. The electron density was contoured at a level of 2.5σ and 3.0σ for aldehyde and vinyl sulfone, respectively. Hydrogen bonds are displayed as thin black lines.

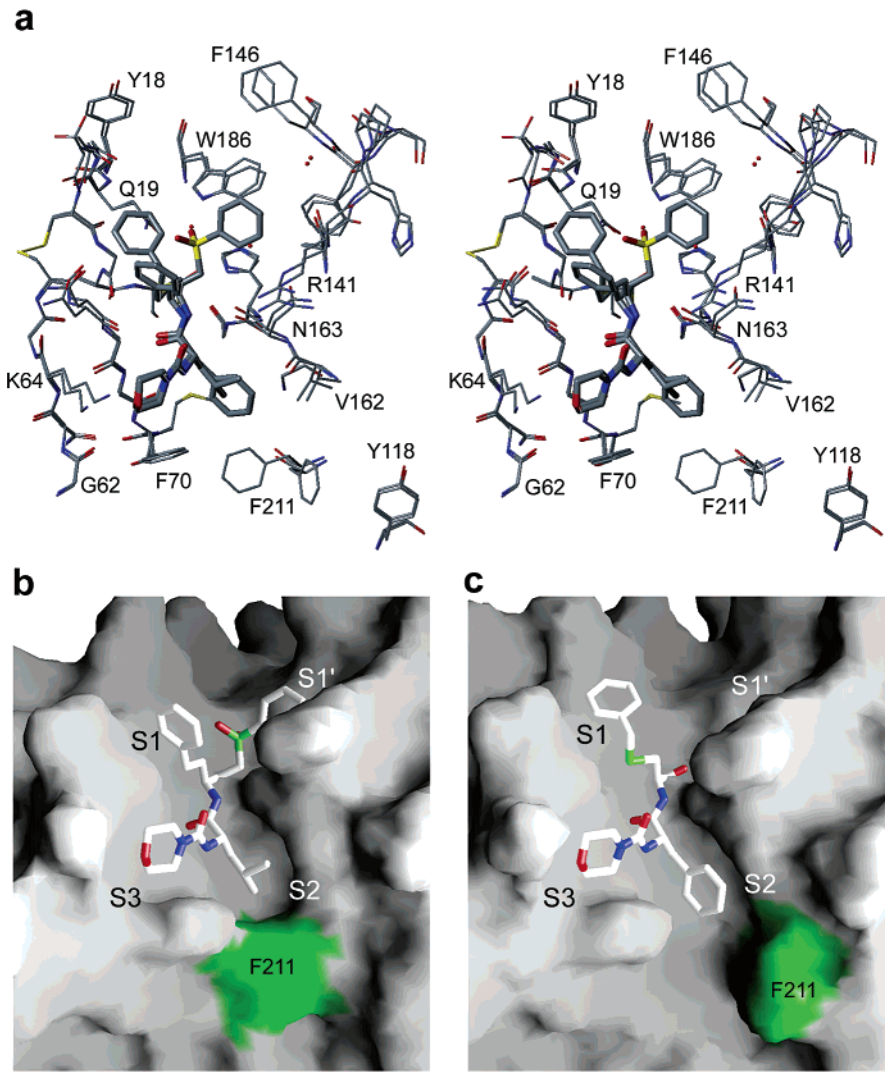

FIGURE 4: Noncovalent interactions between cathepsin S and the bound inhibitor. (a) Stereoview of the binding site region of cathepsin S. The two complexes are superimposed based on all main chain atoms of the enzyme. Inhibitor molecules are shown as thick sticks and protein residues as thin sticks. (b) Steric complementarity between the substrate-binding subsites S1′ to S3 of cathepsin S and the vinyl sulfone inhibitor. (c) The aldehyde inhibitor. The protein is represented by its molecular surface calculated and displayed in GRASP (*33*) after addition of all hydrogen atoms. The molecular surface associated with the side chain atoms of Phe211 residue is colored in green to highlight the different shape of the S2 pocket of cathepsin S upon binding of P2-Leu and P2-Phe of the inhibitors.

both the *S*- and *R*-configurations, with its oxygen atom interacting with the oxyanion hole or with the catalytic histidine residue, respectively.

In the complex with the vinyl sulfone inhibitor, the active site Cys25 thiolate nucleophile of the cathepsin S attacks the mildly reactive vinyl group of the inhibitor at its electrophilic sp^2 carbon atom distal from the SO_2 group. This was structurally observed for vinyl sulfone inhibitors bound to cathepsin K (*18*), cathepsin V (*19*), and cruzain (*28*). The newly formed chiral center C(sp^3) is in the *S*-configuration (Figure 1). The carbon atom vicinal to the SO_2 group points toward the Nδ atom of the active site His164 (Figure 3), indicating the proton transfer from the positively charged His164 to the carbon anion, as proposed for this class of mechanism-based Michael acceptor inhibitors (*29*). As in the case of substrate binding, the alternate configuration is sterically incompatible with the binding site geometry because of the large substituent at the attacked double bond.

Noncovalent Interactions of the Inhibitors. Both inhibitors establish extensive noncovalent interactions with the substrate-binding site of cathepsin S (Figure 4a). The aldehyde inhibitor interacts with subsites S1 to S3 of the enzyme, and the vinyl sulfone inhibitor binds to subsites S1′ to S3 (Figure 4b,c). The peptidic scaffold common to both inhibitors and linking positions P1 through P3 is accommodated in the nonprimed part of the binding cleft. The binding mode of this peptidic backbone is almost identical for the two complexed inhibitors and mirrors closely the canonical substrate-binding mode for cysteine proteases of the papain superfamily. Specific interactions include two hydrogen bonds with Gly69 and one hydrogen bond with the main chain carbonyl of Asn163 of cathepsin S (Figure 3).

The cyclic morpholine moiety at the N-terminal position, common for the two inhibitors, binds to the S3 subsite of the enzyme. The S3 pocket was poorly defined in the previous structure of complexed cathepsin S (*15*), as the cathepsin S specific loop (residues 61−64) was disordered. This subsite is very well-defined in the present structures and shaped by residues Gly68 and Gly69 at its base, by the side chains of residues Lys64 and Phe70 on the sides, and

the backbone atoms of residues Gly62 and Asn63 in the back. The P3-morpholine ring adopts a chair conformation, fills the S3 pocket efficiently, and establishes intermolecular interactions that are very similar for the two inhibitors. More specifically, two aliphatic methylene groups on the same side of the morpholine ring pack against the aromatic ring of Phe70, and one of the methylene groups on the opposite side of the morpholine ring contacts the aliphatic portion of the Lys64 side chain (Figure 4a). The oxygen atom of the morpholine ring is positioned at a distance of 4.1 and 5.0 Å from the positively charged ammonium group of Lys64 in the two complexes, which is too far to establish a hydrogen bond but could lead to a favorable electrostatic interaction.

The S2 subsite is known as the major binding specificity and affinity determinant for the cysteine proteases of the papain superfamily (*14*). The two inhibitors investigated in this study present different moieties to the S2 pocket of cathepsin S, the P2-Phe side chain in the case of the aldehyde inhibitor, and the P2-Leu side chain in the case of the vinyl sulfone inhibitor. The nonpolar nature of these side chains is complementary to the hydrophobic S2 subsite of cathepsin S. The deep S2 pocket of the enzyme is lined by the side chain of Met71 and the methylene groups of Gly137 and Gly165 at its base, with the side chains of Phe70 and Val162 shaping the sides, and the side chain of Phe211 closing the pocket in the distal position. Both the P2-Leu of the vinyl sulfone inhibitor and the bulkier P2-Phe of the aldehyde inhibitor are extremely well-accommodated in the S2 subsite of cathepsin S because of a conformational switch at the level of the Phe211 side chain (Figure 4). This unique structural characteristic of cathespin S and its implications for the specificity against related endopeptidases will be discussed in a separate section below.

Different groups in the two inhibitors occupy the S1 pocket of cathepsin S. The aldehyde inhibitor interacts with its (SBz)Cys group, whereas the vinyl sulfone inhibitor interacts with the Hph group. Both these nonpolar groups share the same general shape in that a phenyl ring is spaced by a linear linker from the main chain of the inhibitor. This geometry appears to particularly suit the shallow S1 subsite, which forms a small depression on one wall of the binding site groove of cathepsin S. Positioning the bulky aromatic ring closer to the main chain of the inhibitor at the bottom of the cleft would cause a steric clash with the enzyme. The S1 subsite is formed mostly by main chain atoms of the enzyme and is lined by residues Gly23, Gly68, Asn67, and the main chain atoms of the Cys22−Cys66 disulfide. The linear, hydrophobic portion of the P1 side chain adopts a very similar, extended conformation in the two inhibitors. The extension of the linker in the (SBz)Cys side chain by a sulfur atom helps project the aromatic ring toward the primed side (Figure 4). Consequently, the bound location of the phenyl ring of the P1 substituent is different in the two inhibitor complexes. The slightly positively charged edge of the phenyl ring establishes electrostatic contacts with carbonyl oxygen atoms (with a negative partial charge) of the protein at both locations. It appears that the (SBz)Cys side chain packs better than the Hph side chain against cathepsin S, which could provide the enthalpic gain necessary to counterbalance the entropic cost of freezing the additional rotatable bond.

Only the vinyl sulfone inhibitor crosses into the S1′ subsite with its phenyl sulfone moiety (Ph-SO_2). One of the oxygen atoms of the SO_2 group makes two hydrogen bonds with the enzyme, with the side chain amide group of residue Gln19 and with the indole amine of Trp186. In the aldehyde inhibitor complex, a water molecule mimics the position and interactions of this sulfone oxygen atom. The other oxygen atom of the SO_2 group is solvent exposed. We can divide the S1′ pocket of cathepsin S into two halves, one proximal to the active site and one more distal. The proximal S1′ subsite is relatively well-shaped and lined by the side chains of residues Trp186 and His164 at its base, with the residues Ala140, Arg141, and Asn163 forming the wall of the pocket. The phenyl ring of the Ph-SO_2 group binds to this proximal pocket of the S1′ subsite, whereas a water molecule occupies this site in the complex with the aldehyde inhibitor (Figure 4). Specific interactions established by the phenyl include stacking with the indole ring of Trp186, hydrophobic contacts with the methyl of Ala140 and the Cγ methylene of Arg141, as well as polar interactions between its edge and three carbonyl oxygen atoms of the protein. We note that in the previous structure of cathepsin S complexed with a vinyl sulfone analogue, the electron density was not sufficient to fit the Arg141 side chain atoms beyond the Cβ (*15*). The phenyl ring of the Ph-SO_2 group does not reach the distal region of the S1′ subsite, which is defined by the main chain atoms of residues His142 and Pro143 and the side chain of Phe146. In this respect, aromatic derivatization of the phenyl ring (e.g., replacement of phenyl with β-naphthyl) would fill the S1′ subsite of the enzyme more completely providing additional packing against the aromatic ring of Phe146. A water molecule is hydrogen-bonded in this region in both complexes of cathepsin S; hence, the desolvation cost of removing this structured water molecule has to be weighed against the gain from additional van der Waals interactions.

Plasticity of the Binding Site. The present structures show that the binding site of cathepsin S displays rigid regions as well as regions of considerable plasticity. Since the peptidic scaffold and the P3-morpholine moiety are common to both inhibitors, we searched for structural differences at the S1′, S1, and S2 subsites of the enzyme (Figure 4a). The S1 subsite adopts a nearly identical conformation after accommodating the (SBz)Cys side chain of the aldehyde inhibior or the Hph side chain of the vinyl sulfone inhibitor. The S1′ subsite appears less rigid and responds to the binding of the Ph-SO_2 group of the vinyl sulfone inhibitor. Binding of the phenyl ring to the proximal S1′ subsite induces subtle conformational changes in the side chains of residues Phe145 and Trp186. In turn, these changes alter the position of residue Phe146, which shows the largest deviation between the two complexes in the primed part of the binding site. This structural plasticity might have important implications for inhibitor design strategies targeting this region.

However, it is the S2 subsite that shows the greatest flexibility because the side chain of Phe211 acts as an adjustable partition (Figure 4). As mentioned earlier, the S2 pocket can accommodate both the P2-Leu side chain of the vinyl sulfone inhibitor and the larger P2-Phe side chain of the aldehyde inhibitor. In the former case, the aromatic ring of Phe211 restricts the size of the S2 pocket and contacts the more buried methyl group of the P2-Leu of the inhibitor (3.7 Å). To accommodate the aromatic ring of P2-Phe in the S2 subsite, the Phe211 side chain swings away by rotations of approximately 120 and 60° of the χ1 and χ2

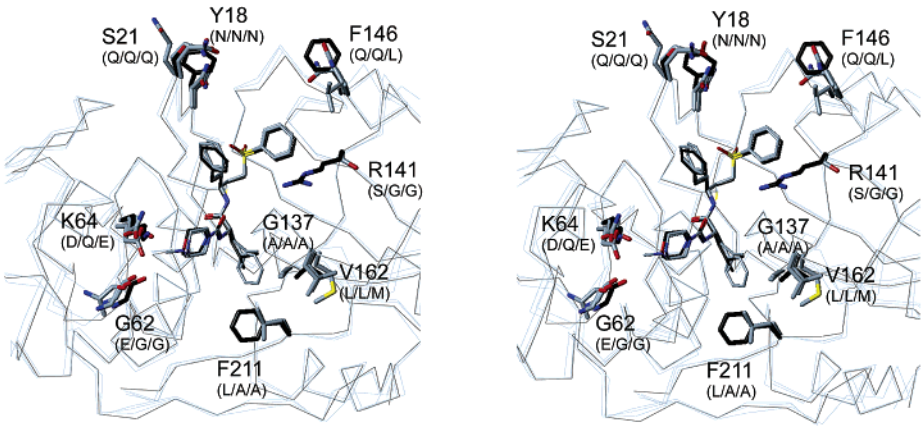

FIGURE 5: Specificity determinants of human cathepsin S as compared to related endopeptidases. Stereoview of the superposition of the present structure of cathepsin S complexed with the vinyl sulfone inhibitor, the crystal structure of cathepsin K complexed with a vinyl sulfone analogue (PDB code 1mem), the crystal structure of cathepsin V complexed with another vinyl sulfone analogue (PDB code 1fh0), and the structure of cathepsin L from the procathepsin L crystal structure (PDB code 1cs8). The alignment is based on the main chain atoms of the homologous residues of the proteins. The three vinyl sulfone inhibitors are displayed as thin sticks. The four aligned protein structures are shown as Cα-trace. Side chains that are unique to the substrate-binding subsites of cathepsin S as compared with those of cathepsins K, V, and L are displayed together with those of the other three endopeptidases as thick sticks. These positions are labeled by the residue name and number in cathepsin S, with the name of the residue found in the other enzymes given in parentheses in the order cathepsin K/cathepsin V/cathepsin L (see also Table 2). The color-coding scheme of the carbon atoms is black for cathepsin S and its inhibitor and gray for the other enzymes and their inhibitors.

angles, respectively. The conformational change of Phe211 side chain also results in a groove that opens the S2 pocket in its inhibitor−distal region (Figure 4c), suggesting that even bulkier, appropriately substituted P2-Phe side chains could be accommodated in the created space. In the new conformation, the aromatic ring of Phe211 establishes specific interactions with the neighboring atoms of the enzyme, including stacking with the aromatic ring of Tyr118 and hydrophobic contacts with the side chain of Val162. The position of the Cζ atom of Phe211 differs by 6.5 Å comparing the two complexes. These conformations of the Phe211 side chain are very clearly defined in the electron density map of their respective structures. This aromatic ring of Phe211 was not well-defined in the previously reported crystal structure of complexed cathepsin S (*15*).

We can relate the structural plasticity of the S2 pocket of cathepsin S with the binding affinity and specificity profiles at the S2 subsite of the enzyme. Inhibition of three related endopeptidases, cathepsins S, K, and L, was measured for a series of vinyl sulfone inhibitors with varying side chains at the P2 position (*17*). The good packing of either P2-Leu or P2-Phe in the S2 pocket of cathepsin S, which is accomplished through the conformational adjustment of Phe211, suggests similar cathepsin S inhibitory potencies for inhibitors carrying these substituents. Indeed, experimental measurements show that the vinyl sulfone inhibitors containing P2-Leu and P2-Phe inhibit cathepsin S with similar second-order rate constants of inactivation, k_{inact}/K_i, of 14.6×10^6 and 5.0×10^6 M^{-1} s^{-1}, respectively, and very similar inhibition constants, K_i, of 13 and 18 nM, respectively (*17*). The S2 subsite of cathepsin S constitutes the binding affinity hot spot of the enzyme since nearly half (45%) of the overall binding affinity is provided by the P2−S2 interactions (*17*). Thus, the plasticity of the S2 subsite of cathepsin S revealed by the present structures is of paramount importance for the rational structure-based inhibitor design process.

The data of Bromme and co-workers (*17*) show that the vinyl sulfone analogues containing P2-Leu and P2-Phe inhibit the related endopeptidase cathepsin K with very different k_{inact}/K_i values of 7.3×10^5 and 6.9×10^3 M^{-1} s^{-1}, respectively, and also very different K_i values of 110 nM and 36 μM, respectively. This highlights the high selectivity of cathepsin K for P2-Leu over P2-Phe. The crystal structure of cathepsin K in complex with a vinyl sulfone inhibitor containing P2-Leu (*18*) shows the tight packing of P2-Leu against the side chain of Leu209, which corresponds to Phe211 of cathepsin S. In binding the P2-Leu of the inhibitor, the side chains of Leu209 of cathepsin K and Phe211 of cathepsin S occupy the same space. The significant loss of binding affinity to cathepsin K by the larger P2-Phe clearly indicates relative rigidity of the S2 subsite of cathepsin K, as contrasted by the plasticity of the S2 subsite of cathepsin S. Several factors might account for the rigidity of Leu209 in the S2 subsite in cathepsin K (e.g., a steric clash with Leu160 (which is Val162 in cathepsin S) and less favorable interactions with Glu115 (Tyr118 in cathepsin S)).

Specificity Determinants. Achieving inhibitory specificity is a particularly challenging task within a given family of enzymes sharing a similar topology of the binding site cleft. This is the case for the family of cysteine endopeptidases such as cathepsins S, K, L, and V, whose structures show a binding site canyon open on both ends. We have compared the binding sites of cathepsin S, cathepsin K (*18*), and cathepsin V (*19*) complexed with vinyl sulfone inhibitors (Figure 5). These inhibitors delineate the substrate-binding mode in the subsites S3 to S1′ and provide a solid structural framework for evaluating further modifications for inhibitor design and optimization. Because the structure of such a complex has not been reported so far for cathepsin L, we include in the comparison the structure of mature cathepsin L derived from the crystal structure of procathepsin L (*30*, *31*).

The vinyl sulfone inhibitors cocrystallized with cathepsins S, K, and V have identical P1′ and P1 substituents and differ slightly in their P2 and P3 substituents. The inhibitors assume nearly identical conformations upon binding to the three

Table 2: Putative Determinants of Cathepsin S Binding Specificity within the Endopeptidase Family of Papain-Like Cysteine Proteases.

subsite	cathepsin S	cathepsins K/V/L
S3	Lys64	Asp/Gln/Glu
	Gly62[a]	Glu/Gly/Gly[a]
S2	Phe211	Leu/Ala/Ala
	Gly137	Ala/Ala/Ala
	Val162	Leu/Leu/Met
S1	None	
S1′ proximal	Arg141	Ser/Gly/Gly
S1′ distal	Phe146	Gln/Gln/Leu
other primed	Tyr18	Asn/Asn/Asn
	Ser21	Gln/Gln/Gln

[a] Located in a loop of variable length in the four endopeptidases. This loop in cathepsin S is three residues longer than in cathepsin K and one residue longer than in cathepsins L and V.

related enzymes, reflecting the conserved shape of the substrate-binding site within the endopeptidase family. Detailed comparison of protein−inhibitor contacts uncovers unique, local structural features of the substrate-binding site of cathepsin S that are not present in the cathepsins K, L, or V. The identified specificity markers of cathepsin S are listed in Table 2 and displayed in Figure 5, showing that except for the S1 subsite there are differences between cathepsin S and other endopeptidases that could be exploited to enhance inhibitor specificity.

The presence of the Lys64 side chain in the S3 subsite of cathepsin S could provide electrostatic interactions that are unique within the endopeptidase family. In the present complexes, the partially negatively charged ether oxygen of the P3-morpholine ring is located in the proximity of the NH_3^+ group of Lys64. The positively charged Lys64 corresponds to an acidic residue in cathepsins K and L and to a neutral but polar residue in cathepsin V. Negatively charged substituents stemming from the cyclic P3 moiety could be designed to strengthen the electrostatic interactions and form hydrogen bonds with the Lys64 side chain of cathepsin S, and therefore, to enhance the specificity against the other endopeptidases.

Another distinctive structural feature of the S3 pocket of cathepsin S is a consequence of a three-residue insertion relative to cathepsin K in the loop between Ser57 and Asn63. This insertion is one residue longer than in cathepsins L and V. The net result is that the S3 pocket of cathepsin S is smaller than that of the other endopeptidases. The carbonyl oxygen atom of Gly62, which protrudes into the S3 pocket closer to the P3 fragment, can be exploited for the design of a specific hydrogen bond from a substituent attached to the P3-ring.

Three residues in the S2 pocket are unique to cathepsin S. As described, the side chain of Phe211 is responsible for the plasticity of the S2 pocket in accommodating P2-Phe relative to the smaller P2-Leu and provides a specificity determinant against cathepsin K, which displays a more rigid Leu209 side chain at the corresponding position. An alanine is found at this position in cathepsins L and V. Accordingly, biochemical data show no difference in specificity between the P2-Leu and P2-Phe for cathepsins S and L (*17*). Two other residues in the S2 subsite might confer specificity toward cathepsin S against the related endopeptidases. Residue Gly137 makes the S2 pocket of cathepsin S deeper than in the other three enzymes, all of which have an alanine in the corresponding position. Conversely, the β-branched Val162 restricts the entrance into the S2 pocket more than in the other enzymes, where a leucine is found at this position in cathepsins K and V and a methionine in cathepsin L. Hence, hydrophobic moieties that utilize and meet these shape requirements could be used as a source of specificity toward cathepsin S.

No structural feature unique to cathepsin S (relative to cathepsins K, L, and V) can be found in the S1 subsite region. However, the guanidinium group of Arg141 side chain, stemming from the proximal region of the S1′ subsite of cathepsin S, reaches toward the top of the S1 pocket. Thus, Arg141 represents a very distinct residue of cathepsin S that can have implications for binding affinity and specificity optimization of both P1′ and P1 substituents. A small residue replaces this Arg141 in the other three endopeptidases, serine in cathepsin K, and glycine in cathepsins L and V. The presence of Arg141 in the S1′-S1 region might contribute to specific cleavage of the MHC class II-associated invariant chain Ii by cathepsin S (*32*).

In the distal region of the S1′ pocket, residue Phe146 of cathepsin S is replaced by glutamine in cathepsins K and V and leucine in cathepsin L. Further into the primed part of the substrate-binding cleft, two residues are also unique to cathepsin S. They are Tyr18 and Ser21 replacing the asparagine and glutamine, which are absolutely conserved in the other three endopeptidases. Although the vinyl sulfone inhibitors investigated here do not contact these residues, further extensions toward the primed subsites could take advantage of the unique interactions that can be formed with these side chains of cathepsin S.

In conclusion, the present crystal structures of inhibitor-bound human cathepsin S provide a solid basis for the molecular design and optimization of inhibitors specific to this enzyme. The structural information reported here allows the identification of putative specificity determinants of cathepsin S. Those unique structural features of the enzyme, including Lys64 and Gly62 of the S3 subsite, Phe211 in the S2 pocket, and Arg141 in the S1−S1′ region, were not delineated in the previously reported structure of the complexed cathepsin S (*15*) because of poor electron density in these regions. While these residues are well-defined in the recently elucidated structure of the inhibitor-free, inactive Cys25Ser cathepsin S mutant (*16*), the information and insight afforded by the structures of the wild-type enzyme complexed with two potent inhibitors has important implications for developing improved, highly specific inhibitors of cathepsin S for the treatment of human diseases.

REFERENCES

1. Kirschke, H., Wiederanders, B., Bromme, D., and Rinne, A. (1989) *Biochem. J. 264*, 467−473.
2. Shi, G. P., Munger, J. S., Meara, J. P., Rich, D. H., and Chapman, H. A. (1992) *J. Biol. Chem. 267*, 7258−7262.
3. Shi, G. P., Webb, A. C., Foster, K. E., Knoll, J. H., Lemere, C. A., Munger, J. S., and Chapman, H. A. (1994) *J. Biol. Chem. 269*, 11530−11536.
4. Riese, R. J., Mitchell, R. N., Villadangos, J. A., Shi, G. P., Palmer, J. T., Karp, E. R., De Sanctis, G. T., Ploegh, H. L., and Chapman, H. A. (1998) *J. Clin. Invest. 101*, 2351−2363.
5. Nakagawa, T. Y., Brissette, W. H., Lira, P. D., Griffiths, R. J., Petrushova, N., Stock, J., McNeish, J. D., Eastman, S. E., Howard, E. D., Clarke, S. R., Rosloniec, E. F., Elliott, E. A., and Rudensky, A. Y. (1999) *Immunity 10*, 207−217.

6. Shi, G. P., Villadangos, J. A., Dranoff, G., Small, C., Gu, L., Haley, K. J., Riese, R., Ploegh, H. L., and Chapman, H. A. (1999) *Immunity 10*, 197−206.
7. Hsieh, C. S., deRoos, P., Honey, K., Beers, C., and Rudensky, A. Y. (2002) *J. Immunol. 168*, 2618−2625.
8. Nakagawa, T., Roth, W., Wong, P., Nelson, A., Farr, A., Deussing, J., Villadangos, J. A., Ploegh, H., Peters, C., and Rudensky, A. Y. (1998) *Science 280*, 450−453.
9. Shi, G. P., Bryant, R. A., Riese, R., Verhelst, S., Driessen, C., Li, Z., Bromme, D., Ploegh, H. L., and Chapman, H. A. (2000) *J. Exp. Med. 191*, 1177−1186.
10. Chapman, H. A., Riese, R. J., and Shi, G. P. (1997) *Annu. Rev. Physiol. 59*, 63−88.
11. Barrett, A. J., and Rawlings, N. D. (1996) *Perspect. Drug Discov. Des. 6*, 1−11.
12. Nagler, D. K., Tam, W., Storer, A. C., Krupa, J. C., Mort, J. S., and Menard, R. (1999) *Biochemistry 38*, 4868−4874.
13. McGrath, M. E. (1999) *Annu. Rev. Biophys. Biomol. Struct. 28*, 181−204.
14. Storer, A. C., and Menard, R. (1996) *Perspect. Drug Discov. Des. 6*, 33−46.
15. McGrath, M. E., Palmer, J. T., Bromme, D., and Somoza, J. R. (1998) *Protein Sci. 7*, 1294−1302.
16. Turkenburg, J. P., Lamers, M. B., Brzozowski, A. M., Wright, L. M., Hubbard, R. E., Sturt, S. L., and Williams, D. H. (2002) *Acta Crystallogr. D58*, 451−455.
17. Bromme, D., Klaus, J. L., Okamoto, K., Rasnick, D., and Palmer, J. T. (1996) *Biochem. J. 315*, 85−89.
18. McGrath, M. E., Klaus, J. L., Barnes, M. G., and Bromme, D. (1997) *Nature Struct. Biol. 4*, 105−109.
19. Somoza, J. R., Zhan, H., Bowman, K. K., Yu, L., Mortara, K. D., Palmer, J. T., Clark, J. M., and McGrath, M. E. (2000) *Biochemistry 39*, 12543−12551.
20. Otwinowski, Z., and Minor, W. (1997) *Methods Enzymol. 276*, 307−326.
21. Brunger, A. T., Adams, P. D., Clore, G. M., DeLano, W. L., Gros, P., Grosse-Kunstleve, R. W., Jiang, J.-S., Kuszewski, J., Nilges, M., Pannu, N. S., Read, R. J., Rice, L. M., Simonson, T., and Warren, G. L. (1998) *Acta Crystallogr. D54*, 905−921.
22. Jones, T. A., Zou, J.-Y., Cowan, S. W., and Kjelgaard, M. (1991) *Acta Crystallogr. A47*, 110−119.
23. Laskowski, R. A., MacArthur, M. W., Moss, D. S., and Thornton, J. M. (1993) *J. Appl. Crystallogr. 26*, 282−291.
24. Menard, R., Carriere, J., Laflamme, P., Plouffe, C., Khouri, H. E., Vernet, T., Tessier, D. C., Thomas, D. Y., and Storer, A. C. (1991) *Biochemistry 30*, 8924−8928.
25. Schroder, E., Phillips, C., Garman, E., Harlos, K., and Crawford, C. (1993) *FEBS Lett. 315*, 38−42.
26. Menard, R., and Storer, A. C. (1992) *Biol. Chem. 373*, 393−400.
27. Delbaere, L. T. J., and Brayer, G. D. (1985) *J. Mol. Biol. 183*, 89−103.
28. Brinen, L. S., Hansell, E., Cheng, J., Roush, W. R., McKerrow, J. H., and Fletterick, R. J. (2000) *Structure Fold Des. 8*, 831−840.
29. Palmer, J. T., Rasnick, D., Klaus, J. L., and Bromme, D. (1995) *J. Med. Chem. 38*, 3193−3196.
30. Coulombe, R., Grochulski, P., Sivaraman, J., Menard, R., Mort, J. S., and Cygler, M. (1996) *EMBO J. 15*, 5492−5503.
31. Groves, M. R., Coulombe, R., Jenkins, J., and Cygler, M. (1998) *Proteins 32*, 504−514.
32. Guncar, G., Pungercic, G., Klemencic, I., Turk, V., and Turk, D. (1999) *EMBO J. 18*, 793−803.
33. Nicholls, A., Sharp, K. A., and Honig, B. (1991) *Proteins 11*, 281−296.

BI027308I